


PROCEEDINGS REPRINT

 SPIE—The International Society for Optical Engineering

Reprinted from

Characterization, Propagation, and Simulation of Sources and Backgrounds II

20–22 April 1992
Orlando, Florida



Volume 1687

Structure of spatial spectra of simulated cloud scenes at infrared wavelengths

Jerry Tessendorf
Daniel Weston
Lisa Taylor

Areté Associates, PO Box 6024, Sherman Oaks, CA 91413

ABSTRACT

Longwave infrared imagery of cloud fields are examined in terms of their power spectral density (PSD). In order to systematically investigate the dependence of the PSD on viewing conditions, a cloud scene simulator is employed to generate images of a simulated cloud field. The cloud field is fully three dimensional and is described by is fluctuating temperature and liquid/ice water content fields. The imaging process accurately calculates the spatially varying attenuation of blackbody emission. Several views of a single cloud field are examined to study the effect of viewing angle on the image PSD. Zenith views produce isotropic PSDs, while nearly horizontal views contain a large amount of foreshortening and a correspondingly anisotropic PSD. One possible component of the foreshortening is simply geometric and can be estimated and compared to the simulation output. We find that geometrically induced foreshortening does not describe the PSD effects observed in the simulation for the relatively thin cirrus-like cloud simulated here. Possibly this indicates that the three-dimensional cloud structure is more important in some views than in others when there are large fluctuations in the cloud optical properties. We are pursuing a more quantitative description of this behavior.

1. INTRODUCTION

A common method of characterizing environmental clutter in imagery is in terms of the Power Spectral Density (PSD) of the images. The motivation for examining the PSD derives from signal processing concepts, in which clutter may be suppressed in an optimal sense by whitening the image with filter coefficients based on the PSD. This approach applies to many disciplines, for example optical imagery and time series analysis. It seems therefore, to be a natural starting point for characterizing clouds as clutter in infrared images.

We can imagine however, that many aspects of clouds should limit the value of the PSD, or at least complicate its use, in describing cloud images. For example, the PSD has the simple interpretation as the Fourier transform of the space-lagged correlation function when the statistics are homogeneous. Cloud scenes however, can be extremely inhomogeneous when the cloud field is broken or optically thin in places. In this regard the PSD is still useful as a descriptor of the statistically homogeneous component of the scene, or if the inhomogeneity is in some sense small.

The qualitative structure of clouds in an image can also depend strongly on the angle at which the cloud is viewed, even assuming a homogeneous cloud field is present. This is because the footprint size and shape of a camera pixel depends on the camera viewing angle with respect to the "cloud face." In addition, clouds are fundamentally three-dimensional objects, and the radiance at the camera includes volumetric emissions from within some absorption-limited volume. If there are significant spatial variations in cloud structure over distances less than or comparable to one optical depth, viewing the cloud from two different angles will give different perspectives of the three-dimensional variations within the cloud, and different optical depths to those structures.

In this paper we begin an on-going program of examining the spatial/statistical structure of cloud scenes in long-wave infrared imagery in order to evaluate the connection between cloud structure and appearance in images. As a starting point we are using the PSD to characterize cloud spatial structure as a function of viewing angle on the cloud bottom. Because there is little infrared image data gathered to examine this behavior, we are using a cloud scene simulator developed under the Infrared Analysis, Measurements, and Modeling Program (IRAMMP) to aid in the analysis. This model was developed specifically to be able to address these kinds of issues, and is described in Section 2. In comparisons with infrared cloud scenes collected by the IRAMMP sensor, the PSD structure of the simulator is consistent with that of the IRAMMP data.

In Section 3 a set of images of a single three-dimensional cloud field is analyzed as a function of the view angle. As the view angle changes from a zenith view to a near horizontal view, the PSD of the images changes from isotropic to elongated in the elevation direction. This foreshortening may be due simply to geometric changes because the camera pixel footprint elongates on the "cloud bottom," and/or because of changes in the way the three-dimensional cloud structure is viewed. Geometrically induced foreshortening can be estimated and a predicted PSD is compared to the observed PSD. This shows quantitatively that much of the actual foreshortening is due to the three-dimensional character of the cloud and not geometric foreshortening. Section 4 contains a discussion of the analysis results, and suggested direction for continued work.

2. CLOUD SCENE SIMULATOR

In order to examine the consequences of three-dimensional cloud structure in infrared images, the cloud scene simulator generates a realization of a three-dimensional cloud. The quantities of primary interest in describing the cloud are the temperature field $T(\bar{x})$ and absorption coefficient $a(\bar{x})$ at all points in the cloud. At this stage of simulator development we are not including scattering processes or solar or earthshine, although we plan to implement appropriate algorithms for these processes in the near future. Since we are interested in wavelengths in the 8-12 μm range, it is reasonable to begin our study with only absorption and thermal emission.

2.1 CLOUD REALIZATION

The fields of temperature and absorption are generated from a statistical prescription while preserving microphysical constraints. The temperature is a combination of a mean profile containing information on the lapse rate and inversion if desired, plus a fluctuation component:

$$T(\bar{x}) = T_0(z) - \xi(\bar{x}) \sigma_T(z) \quad (1)$$

where $T_0(z)$ is the mean profile, $\sigma_T(z)$ is the standard deviation of temperature, which can be altitude dependent, and $\xi(\bar{x})$ is a field of gaussian random numbers with zero mean and a standard deviation of 1. Since fluctuations in the cloud field are due to an underlying turbulent motion, the fluctuations $\xi(\bar{x})$ are built to have a three-dimensional spectrum of the form

$$\left\langle \left| \tilde{\xi}(\bar{q}) \right|^2 \right\rangle \propto (q_0^2 + q^2)^{-r/2}, \quad (2)$$

where \bar{q} is a three-dimensional wavevector, q_0 is a low-wavenumber cutoff, and r is the exponent of a large- q power law.

The absorption field is generated from a field of ice or liquid water content $\rho(\bar{x})$. Distinct from the temperature field, ρ is given a log-normal form

$$\rho(\bar{x}) = \rho_0(z) \exp \left\{ \xi(\bar{x}) \sigma_\rho(z) - \frac{\sigma_\rho^2(z)}{2} \right\}, \quad (3)$$

where $\rho_0(z)$ is the mean profile of water content, $\sigma_\rho(z)$ is the profile of standard deviation of the log-normal fluctuations, and $\xi(\bar{x})$ is the same fluctuation field as used for the temperature. From the water/ice content, the absorption is generated as

$$a(\bar{x}) = C_1 \rho(\bar{x})^{C_2}. \quad (4)$$

Many researchers have noted that $C_2 = 1$ in long-wave bands^{1,2}, and from in-situ measurements of marine stratus, Noonkester reported the fit³

$$\begin{aligned} C_1 &= 381 \\ C_2 &= 1.142 \end{aligned}$$

where $\rho(\bar{x})$ is in units of g/m^3 and $a(\bar{x})$ is in units of km^{-1} . For this study we used these values, recognizing that they may not apply in many situations.

2.2 IMAGING

The camera is imagined to be a focal plane array located at position \bar{x}_c , and looking in direction \hat{n}_c . Each pixel in the array views a direction slightly different than \hat{n}_c . The radiance received at pixel (ij), which views radiance coming from direction \hat{n}_{ij} is the sum of cloud and atmospheric contributions. The cloud contribution to the radiance is

$$L_{cloud}(\bar{x}_c, \hat{n}_{ij}) = \int_0^{\infty} ds a(\bar{x}_c - \hat{n}_{ij}s) B(T(\bar{x}_c - \hat{n}_{ij}s)) \exp\left\{-\int_0^s ds' a(\bar{x}_c - \hat{n}_{ij}s')\right\}, \quad (5)$$

where B is the blackbody radiance in the band at temperature $T(\bar{x}_c - \hat{n}_{ij}s)$. In addition, atmospheric emission and attenuation make the radiance at the camera pixel ij

$$L_{ij} = L_{path} + \tau_{path} \left[L_{cloud}(\bar{x}_c, \hat{n}_{ij}) + \tau_{cloud}(\bar{x}_c, \hat{n}_{ij}) L_{sky} \right], \quad (6)$$

where L_{path} is the atmospheric emission between the cloud and camera, τ_{path} is the atmospheric transmission along the path, and L_{sky} is the atmospheric emission from the sky beyond the cloud. These three quantities are provided by LOWTRAN. The quantity τ_{cloud} is the transmission of the sky radiance through the cloud:

$$\tau_{cloud}(\bar{x}_c, \hat{n}_{ij}) = \exp\left\{-\int_0^{\infty} ds a(\bar{x}_c - \hat{n}_{ij}s)\right\}. \quad (7)$$

Equations (5) - (7) amount to a ray tracing algorithm through the volume of the cloud realization. Our implementation of the ray tracing accounts for the changes in pixel footprint size on the cloud as the viewing direction changes. It also contains logic for tracing through multiple cloud fields, although that is not used here.

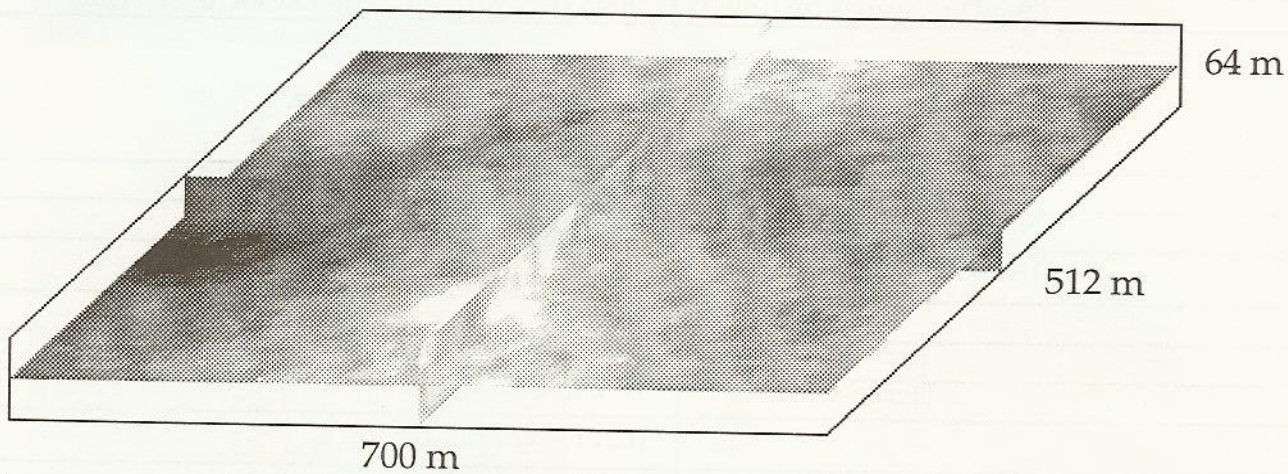


Figure 1. Visualization of a segment of the fluctuation field $\xi(\bar{x})$. Three planar slices through the field are shown.

3. SIMULATED SCENES

A fluctuation field $\xi(\bar{x})$, temperature field $T(\bar{x})$, and absorption field $a(\bar{x})$ were generated using the parameters listed in Table 1. A high altitude cirrus-like parameterization was chosen so that the cloud would be optically thin for the zenith viewing direction, but optically thick for views near horizontal along the long axis of the cloud. This arrangement should emphasize the importance of volumetric effects in the image PSD. The fluctuation field $\xi(\bar{x})$ is depicted in Figure 1, where several planar slices through a segment of the field are used in the visualization.

Images were generated for a camera with parameters shown in Table 2. Nine images were generated for view angles ranging from $\theta=0^\circ$ (viewing straight up at the center of the cloud) to $\theta=80^\circ$ (10° from horizontal) in 10° increments. The images are centered on the same location on the cloud bottom by raising the location of the camera appropriately. Grayscales of those at 0° , 30° , 60° , and 80° are shown in Figure 2. The zenith view image looks isotropic in the fluctuations. As the view angle is increased, the images appear smoother, and additional cloud material comes into view. At 60° significant changes in the image appearance are present, and at 80° the image shows horizontally oriented clutter.

Table 1. Parameters for Cloud Simulation

Parameter	Value
Mean Liquid/Ice Water Content Lapse Rate	0.1 (g/m ³)/km
Standard Deviation of Liquid/Ice Water Content (fraction of Mean Content)	3
Height of Cloud Bottom	10 km
Height of Cloud Top	10.064 km
Width of Cloud	512 meters
Length of Cloud	8.196 km
Mean Temperature at Bottom of Cloud	228 K
Mean Temperature Lapse Rate	7 K/km
Standard Deviation of Temperature	0.4 K
Cloud Resolution Cell Size	4 m X 4 m X 4 m
Cutoff q_0	0 (No cutoff)
Cloud Dimensions (in Cells)	2048 (Length) X 128 (Width) X 16 (Height)

Table 2. Parameters for the Camera and Atmosphere.

Parameter	Value
Number of Camera Pixels	128 X 128
Single Pixel Field of View	400 μ rad X 400 μ rad
MTF	None
Instrument Noise	None
Distance to Cloud	10 km
L_{path}	0.2117 W / m ² str μ m
L_{sky}	0.724 W / m ² str μ m
τ_{path}	0.892

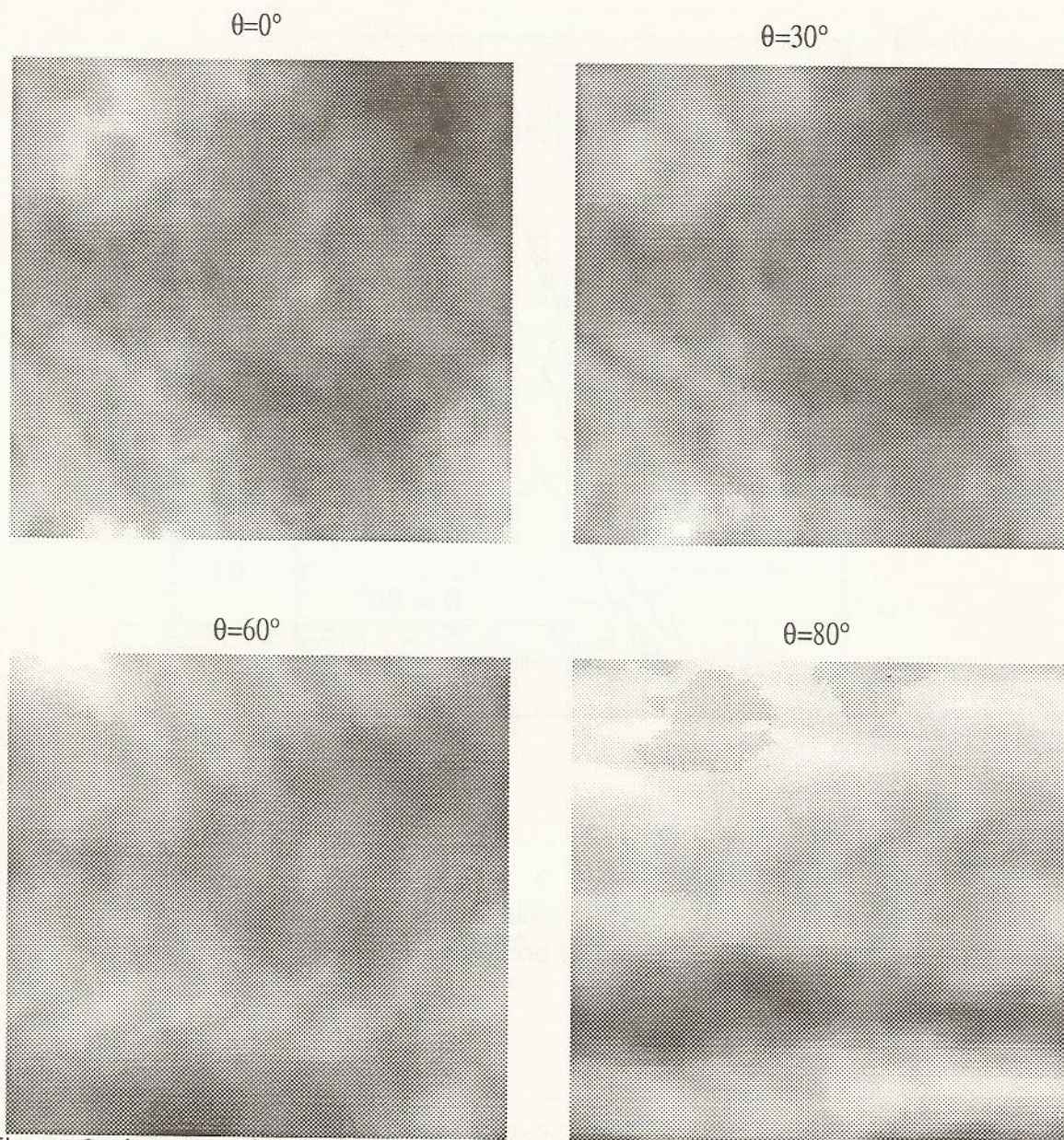


Figure 2. Images of a single cloud field from several different view directions. The view angle θ is with respect to zenith.

The PSDs for the images in Figure 2 are shown as contour plots in Figure 3. Each plot uses the same set of contours, spaced 10dB apart. As expected from the images, the PSD at $\theta=0^\circ$ is isotropic, whereas the PSD at $\theta=80^\circ$ is elongated in the elevation direction. At 30° , there is no obvious evidence of foreshortening in the PSD, but at 60° the large scale structure shows some evidence of the effect. In order to show the foreshortening of the spectrum more quantitatively, horizontal and vertical slices of the PSDs are shown in Figure 4. The slices at the zenith view are the same magnitude and rolloff over the six decades from the largest to the smallest scales. The slices at $\theta=80^\circ$ however, are clearly different magnitude, and the rolloff of the vertical slice may also be slightly faster. Least square fits to a power law

$$P(k) = A k^{-\tau}$$

for the slices in the wavenumber region $100/\text{rad} \leq k \leq 1000/\text{rad}$ yielded the coefficients and goodness of fit shown in Table 3. The differences between the values for the horizontal and vertical slices for $\theta=0^\circ$ reflect the level of estimation error in fitting

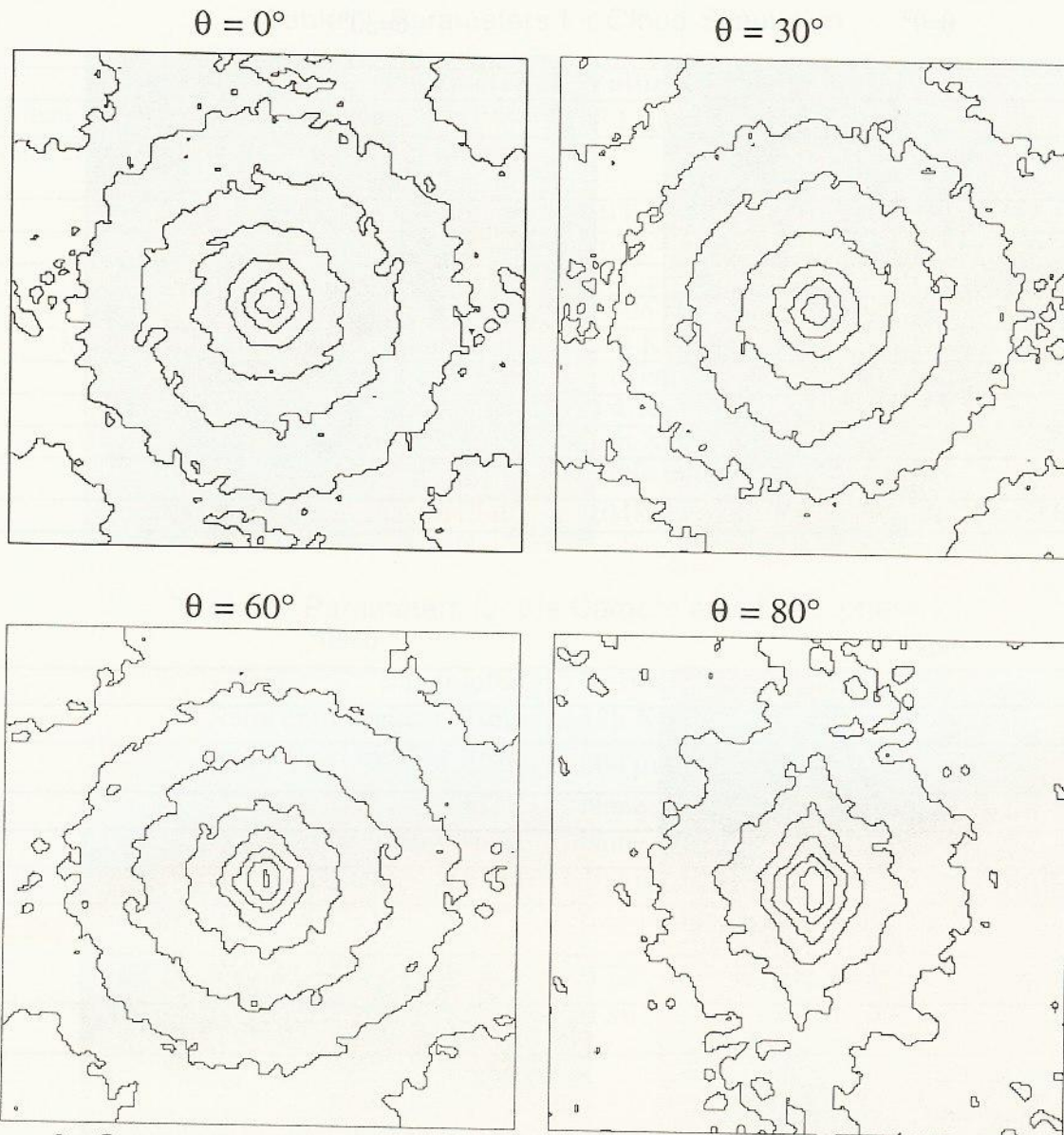


Figure 3. Contour plots of the image PSDs at several viewing angles. The contour levels spaced 10 dB, and the same set is used in all of the plots.

the parameters. The differences in the parameter values for the $\theta=80^\circ$ case are much larger and reflect the true anisotropy of the image.

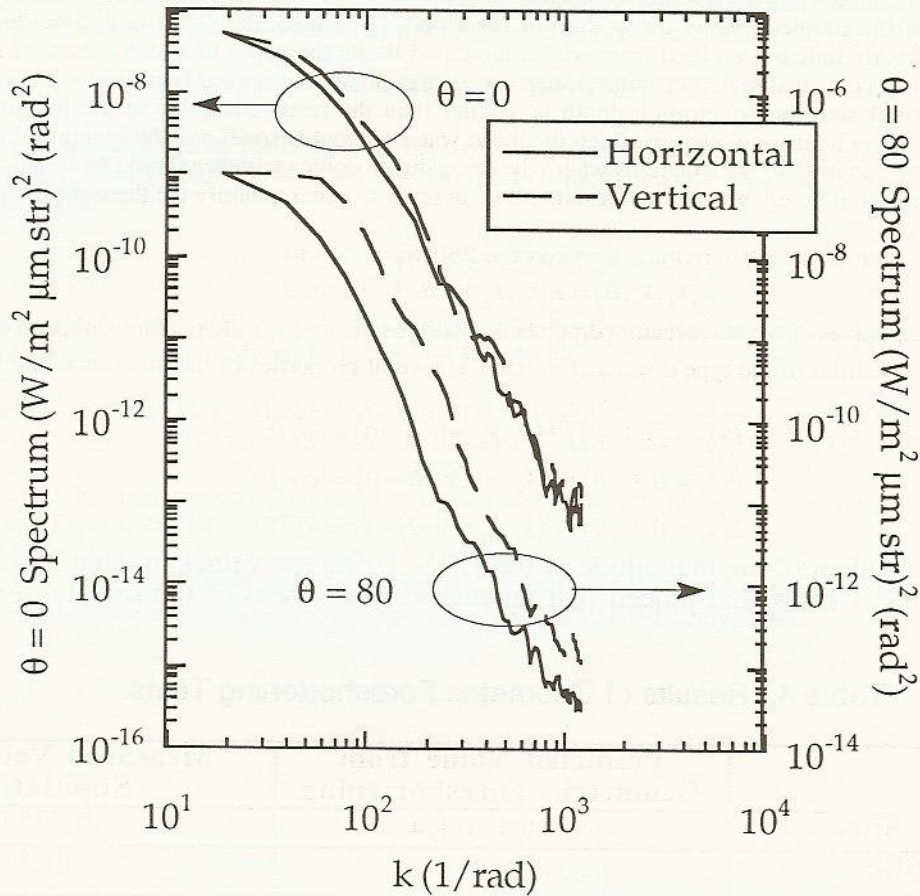


Figure 4. Horizontal and vertical slices through the PSDs in Figure 2 at $\theta=0^\circ$ and 80° . The scales are displaced to better display the separate PSDs.

Table 3. Parameters from Least Squares Fits of Spectral Slices to Power Law

Spectral Slice	A $(W/m^2 \text{ mm str})^2 (\text{rad})^{2-r}$	r	Regression Coef.
$\theta=0^\circ$ Horizontal	1.08	4.33	0.997
$\theta=0^\circ$ Vertical	2.40	4.42	0.995
$\theta=80^\circ$ Horizontal	0.0814	4.10	0.989
$\theta=80^\circ$ Vertical	27.5	4.74	0.997

4. GEOMETRIC FORESHORTENING

One possible source of the anisotropy in the PSD at large θ is geometric foreshortening. If the imaged scene were

effectively two-dimensional, then as the view angle changes the image is simply contracted in the direction of the change, due to the increasing size of the footprint along the bottom of the cloud. Of course, the cloud is a three-dimensional object. Attenuation of the blackbody radiance emitted from within the cloud limits the depth to which a camera is sensitive to the cloud structure, so that it is conceivable that in some circumstances the cloud does appear two-dimensional because there are no holes in the cloud field, and the penetration depth is smaller than the resolved scales in the imaging. In this work however, we have selected a cloud simulation in which the mean water content is small and the lognormal fluctuations about the mean are large, in order to investigate situations where the three-dimensional character should be large. We can however, examine the predicted impact of purely geometric foreshortening, in order to better quantify the three-dimensional effects.

Assuming pure geometric foreshortening, the stretched PSD has the form

$$P(k_x, k_y, \theta) = P(k_x, k_y, \cos \theta, \theta = 0) \cos \theta \quad (8)$$

where k_x, k_y are the components of the wavevector perpendicular and parallel to the camera plane direction of angular change. Assuming a power-law spectrum of the type discussed in table 3, several properties of the horizontal and vertical slices are immediately testable:

Horizontal Slice: $P(k_x, k_y = 0, \theta) / P(k_x, k_y = 0, \theta = 0) = \cos \theta \quad (9)$

Vertical Slice: $P(k_x = 0, k_y, \theta) / P(k_x = 0, k_y, \theta = 0) = (\cos \theta)^{1-r} \quad (10)$

Ellipticity: $P(k_x = 0, k_y, \theta) / P(k_x, k_y = 0, \theta) = (\cos \theta)^{-r} \quad (11)$

These tests are independent of the magnitude of the PSD. Using the values in table 3, the results of the tests reported in table 4 show that indeed that geometric component of the foreshortening is not the dominant effect.

Table 4: Results of Geometric Foreshortening Tests.

Test	Predicted Value from Geometric Foreshortening	Measured Value from Simulation
Horizontal Slice	$\cos(80^\circ) = 0.174$	0.0757
Vertical Slice	$(\cos(80^\circ))^{1-4.2} = 271$	11.5
Ellipticity	$(\cos(80^\circ))^{-4.2} = 1500$	338

Another measure of the geometric component of the foreshortening is the ratio of the observed PSD to one predicted by foreshortening based on the PSD at $\theta=0$. The PSD at $\theta=0$ shown in figure 5(a) was used to construct the predicted PSD in figure 5(b). The observed PSD is in figure 5(c), and the ratio of observed to predicted PSDs is shown in figure 5(d) as a contour plot of the ratio. A \log_{10} scale is used to label the contours, so that the 0 contour is a ratio of unity, and the -2 contour is a ratio of 0.001. From figure 5, the foreshortening impact in the IR images causes the PSD to rolloff much faster than expected from just the two-dimensional geometric effect. One possible explanation is that at large angles, the cloud is mostly optically opaque, whereas the zenith view sees an optically thin cloud. The large angle view integrates the thermal emissions over several fluctuation lengths, and for most regions of the scene does not see contributions from the sky behind the cloud. In contrast, the zenith view integrates over less than a single fluctuation length scale, and has sky contributions at every pixel. The stronger importance of integrating through the cloud volume at larger angles may "smooth" the cloud in some sense, which causes the PSD to roll off faster. Additional work underway will clarify this description and quantify the mechanism for the observed structure.

4. DISCUSSION

We have shown that the structure of PSDs of cloud scenes in the longwave infrared is sensitive to the angle with respect to the bottom of the cloud field at which it is viewed. This is due not just to changes in the geometry of viewing the bottom, but is strongly affected by the underlying three-dimensional structure of the cloud field. It is important to understand this effect at an analytical level in order to properly model PSDs of cloud scenes. Additional simulation work would also provide important information. For example, if the cloud were highly opaque at any viewing angle, corresponding for example to a thick cumulostratus deck, then the three-dimensional character should be suppressed more in the PSD. In this case the geometric foreshortening approach might work better. However, even though the cloud would be optically very

thick, it is likely that with sufficiently high resolution, the sensor will see fundamentally three-dimensional consequences. This behavior at small imaged scales is predicted by a simple linear response model for PSDs developed earlier⁴.

ACKNOWLEDGMENTS

This work was supported by the Infrared Analysis, Measurements, and Modelling Program (IRAMMP) of the Office of Naval Technology. We would like to thank Mr. Douglas Crowder and Dr. Morton Farber for their assistance in the preparation of this paper.

REFERENCES

1. A.W. Gertler and R. L. Steele, "Experimental Verification of the Linear Relationship between IR Extinction and Liquid Water Content of Clouds," *J. Appl. Meteorol.*, **19**, 1314-1317, 1980.
2. G. L. Stephens, S.-C. Tsay, P. W. Stackhouse, Jr., and P. J. Flatau, "The Relevance of the Microphysical and Radiative Properties of Cirrus Clouds to Climate and Climate Feedback," *J. Atmos. Sci.*, **47**, 1742-1753, 1990.
3. V. R. Noonkester, "Extinction coefficients calculated from aerosol spectra measured in a convective marine boundary layer with stratus," *Appl. Optics*, **20**, 1275-1277, 1981.
4. L. Thebaud, M. Farber, S. Hemple, and J. Tessendorf, "Statistics of IR Cloud Images - A Modeling Approach," *Cloud Impacts on DOD Operations and Systems 1991 Conference (CIDOS-91)*, 9-12 July, 1991.

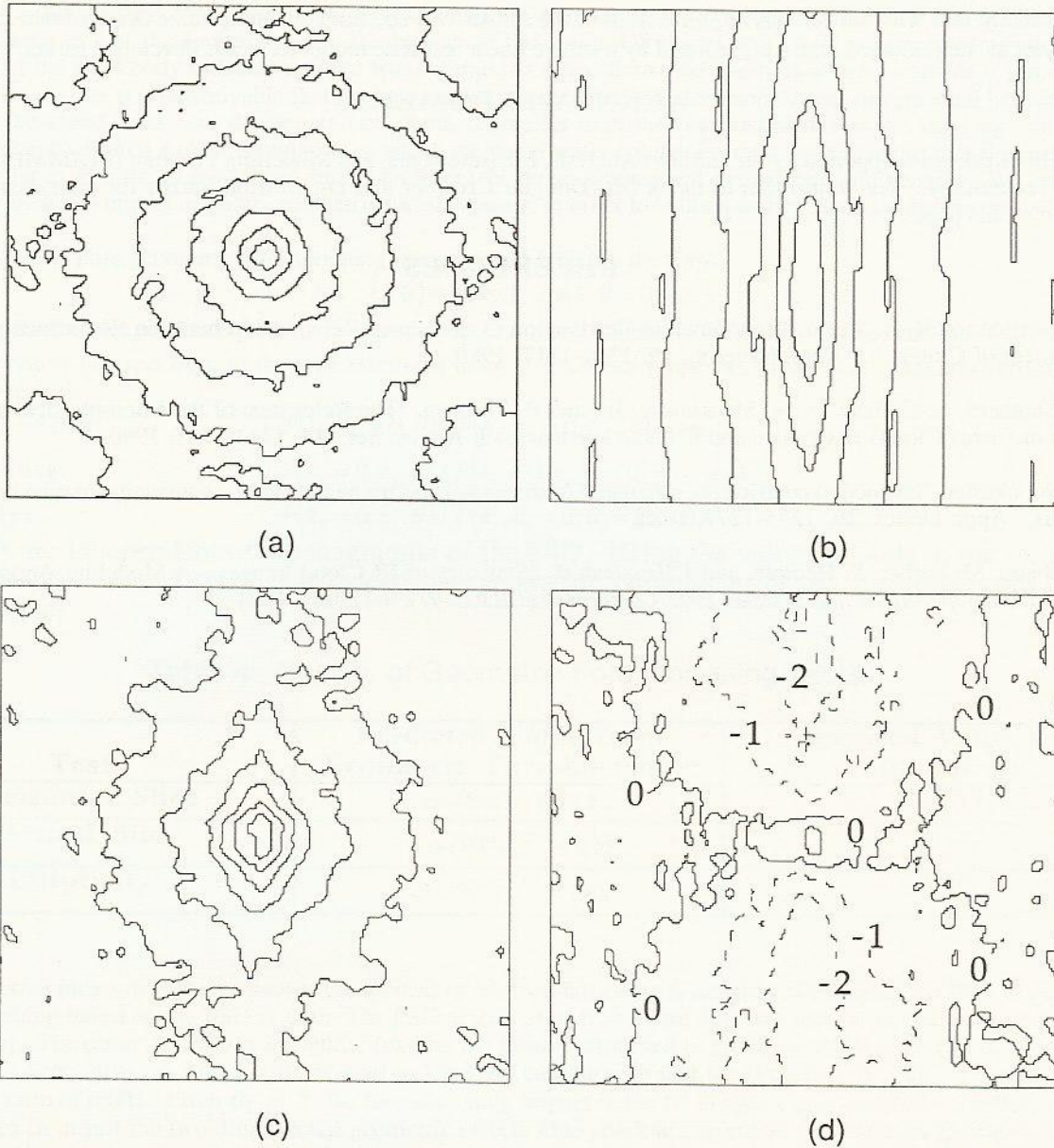


Figure 5. Predicted magnitude of geometric foreshortening. (a) The PSD at $\theta=0$ from the simulation; (b) The PSD at $\theta=80$ predicted by geometric foreshortening; (c) The PSD at $\theta=80$ observed in the simulation; (d) The ratio of the observed to predicted PSDs at $\theta=80$.